JOURNAL OF GEOPHYSICAL RESEARCH, VOL. 107, NO. B3, 10.1029/2000JB000049, 2002

Thermal structure of the North American uppermost mantle inferred from seismic tomography

Saskia Goes and Suzan van der Lee
Institute of Geophysics, ETH Zurich, Zurich, Switzerland

Received 8 November 2000; revised 24 August 2001; accepted 25 August 2001; published 23 March 2002

[1] We map the thermal state of the North American mantle between depths of 50 and 250 km by inverting *P* and *S* velocities of three recent seismic tomographic models. In the well-resolved regions, temperatures derived from *P* velocities agree with those derived from *S* velocities within the estimated uncertainties, and generally, the seismic temperatures are in agreement with those inferred from surface heat flow. Adiabatic mantle temperatures are found as shallow as 50 km under most of the Basin and Range. Warm, subsolidus mantle and known crustal structure can account for the high average elevation and large-scale variations in topography of western North America. In the cratonic mantle beneath the stable eastern part of North America, temperatures at 50–100 km are on average 500°C cooler than under the tectonic western part of the continent and adiabatic mantle temperatures are not reached until 200–250 km depth. To balance the effect on topography of the thermally implied density increase for the North American craton, we infer a compositionally induced density decrease equivalent to a 1% depletion in iron over a depth interval of 50–250 km. In regions where T_P differs significantly from T_S we drop our assumption that variations in seismic velocity are only due to thermal structure. A discrepancy between T_P and T_S between 50 and 150 km depth under the Cascades and the Gulf of California can be accounted for by the presence of 1 to 2 vol % of fluids and/or melt. Another such discrepancy beneath Wyoming remains enigmatic. *INDEX TERMS:* 8180 Tectonophysics: Tomography; 9350 Information Related to Geographic Region: North America; 8110 Tectonophysics: Continental tectonics—general (0905); 7218 Seismology: Lithosphere and upper mantle; *KEYWORDS:* Temperature, Lithosphere, *S* velocity, *P* velocity, Heat flow, North America

1. Introduction

[2] The geology of the North American continent and the geophysical properties of the lithosphere and shallow mantle grossly divide the continent into a tectonically active western part and a stable eastern part. The dividing line between east and west coincides more or less with the Rocky Mountain Front (Figure 1). This division is also present in global seismic velocity models where low upper mantle velocities are found under the western United States and high-velocity upper mantle underlies eastern North America [e.g., *Grand*, 1994]. Furthermore, the western United States is characterized by high surface heat flow [*Morgan and Gosnold*, 1989], low-amplitude magnetic anomalies and negative long-wavelength Bouguer gravity [*Kane and Godson*, 1989], thin crust [*Braile et al.*, 1989; *Mooney et al.*, 1998] and low crustal P_n and S_n velocities [*Braile et al.*, 1989; *Nolet et al.*, 1998]. All these properties indicate a warm uppermost mantle. High temperatures in the uppermost mantle have also been held responsible for the high elevations of western North America [e.g., *Kane and Godson*, 1989; *Kaban and Mooney*, 2001]. In contrast, the eastern part of the continent is characterized by low relief, low to very low surface heat flow [*Morgan and Gosnold*, 1989], significant short-wavelength magnetic and gravity anomalies which seem to correlate with old (~1 Ga) tectonic features [*Kane and Godson*, 1989], thick crust, and high crustal and shallow mantle velocities [*Braile et al.*, 1989; *Mooney et al.*, 1998; *Nolet et al.*, 1998].

[3] The last tectonic activity in eastern North America is related to the Appalachian orogeny (450–350 Ma). The interior United States has been stable since the Grenville orogeny and the formation of the Midcontinent Rift around 1 Ga. This rift runs from the central plains in Kansas NNE to Lake Superior and continues under Michigan. The Superior province was formed around 2.7 Ga. The far inland deformation of the western United States during the Laramide orogeny (75–35 Ma) reached as far west as the Archean Wyoming craton. Laramide compression is generally attributed to basal traction during a phase of very shallow subduction [e.g., *Atwater*, 1989]. At ~40 Ma, Basin and Range extension started and subduction steepened and was gradually replaced by Pacific-North America transform motion, resulting in a growing slab gap [*Dickinson and Snyder*, 1979; *Atwater*, 1989]. Subduction is still continuing today under the coast of Oregon and Washington and Central America. The Yellowstone caldera has the highest continental heat flow values measured anywhere and is strongly volcanically active. Yellowstone volcanism is thought to be associated with a mantle plume, which has, over the last 16 Myr, formed a hot spot track in the Snake River Plain. Recent (Holocene) volcanism is documented all over the U.S. west of the Rocky Mountain front [*Simkin and Siebert*, 1994].

[4] *Humphreys and Dueker* [1994a] used *P* wave velocity anomalies [*Humphreys and Dueker*, 1994b] and a qualitative comparison with surface heat flow and topography to estimate temperature, composition and amount of melt in the shallow mantle under the western United States. They proposed a model of a cool thermal lithosphere under the coastal regions and a lithosphere affected by melting processes under the interior western United States. They interpreted low-velocity anomalies under the Basin and Range to be caused by the presence of 1–3% of melt, while high-velocity anomalies were attributed to iron depletion by melting processes. They held the density reduction associated with melt and iron depletion responsible for the high topography of the western United States. Most other temperature estimates for the

0148-0227/02/2000JB000049$09.00

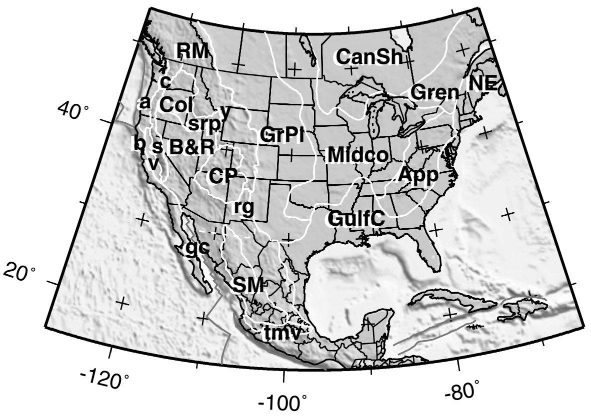

Figure 1. Map of North America showing physiographic provinces (white lines), oceanic plate boundaries (dark gray lines) and political boundaries (thick lines, national borders; thin lines, state borders). The following regions are referred to in the text: a, Oregon/Washington coastal region; App, Appalachians; b, California coastal region; B&R, Basin and Range Province; c, Cascade Range; CanSh, Canadian Shield; Col, Columbia Plateau; CP, Colorado Plateau; gc, Gulf of California; Gren, Grenville Province; GrPl, Great Plains; GulfC, Gulf of Mexico Coast Plains; Midco, Midcontinent; NE, New England Province; rg, Rio Grande Rift; RM, Rocky Mountain Province; s, Sierra Nevada; SM, Sierra Madre Occidental; srp, Snake River Plain; tmv, Trans-Mexican Volcanic Belt; v, California Great Valley; and y, Yellowstone Caldera. The dashed white line mark the southern boundary used for determining average temperatures for the Basin and Range.

North American lithosphere are based on the analysis of surface heat flow observations. For example, high and nonsteady state lower crustal temperatures were inferred under the Basin and Range and the Rio Grande Rift [*Lachenbruch et al.*, 1994; *Decker*, 1995; *Artemieva*, 1996]. Petrological data and surface heat flow modeling predicted Moho temperatures of 800–1000°C under the Colorado Plateau and most of the southern Rocky Mountains [*Decker*, 1995; *Artemieva*, 1996]. A global study of temperatures from heat flow under Precambrian areas [*Artemieva and Mooney*, 2001] gives temperatures as low as 500°C at 50 km depth under the North American craton and a thermal lithospheric thickness (defined as the depth of the 1300°C isotherm) of 200–250 km.

[5] In this paper we map the thermal state of the uppermost North American mantle by inverting seismic *P* and *S* velocities for temperatures between depths of 50 and 250 km. Our study is motivated by the availability of improved models of the seismic structure of the upper mantle under North America and the availability of both *P* and *S* velocity models. We compare temperature estimates from *P* and *S* velocities with each other and with lithospheric temperatures inferred from surface heat flow. Initially, we assume that variations in seismic velocities are solely due to variations in mantle temperature. The comparison between temperatures independently obtained from *P* and *S* velocities and from heat flow allows us to test this assumption and evaluate whether additional factors, e.g., the presence of fluids or anisotropy, are influencing seismic velocities of the shallow North American mantle. Three velocity models are used, the North American *S* velocity model NA00, the global *P* velocity model BSE-NL [*Bijwaard and Spakman*, 2000] and the western U.S. *P* velocity model of Dueker and coworkers [*Dueker*, 1999; *Dueker et al.*, 2001]. The temperatures from surface heat flow are from published geothermal modeling studies as well as from one-dimensional (1-D) steady state modeling using surface heat flow data from the global heat flow database [*Pollack et al.*, 1993]. Because of coverage and resolution, only the *S* velocity model can be analyzed for temperature under the North American continent from southern Canada to Mexico. A comparison with heat flow and *P* velocities from BSE-NL is made where possible. A more detailed of analysis is made of temperatures under the western United States, where the tomographic models have the best resolution and the model of Dueker provides additional constraints on *P* wave velocity.

2. Seismic Velocity Models

[6] NA00 (S. van der Lee et al., manuscript in preparation, 2001) is based on waveforms from *S* and surface wave trains from 794 vertical component, broadband seismograms, including those used for NA95 [*van der Lee and Nolet*, 1997b], which were jointly inverted for 3-D *S* wave velocity structure and Moho depth. In NA00 trade-offs between Moho depth, crustal and subcrustal velocities are reduced by including independent constraints on Moho depth from the database compiled by *Chulick and Mooney* [1998]. Although NA00 does not significantly alter the waveform fits compared to model NA95, it does provide a better estimate of subcrustal velocities, which is important in estimating lithospheric temperatures. The minimum horizontal resolution length is around 200 km. Some smearing along the mostly horizontal wave paths occurs under the Atlantic Ocean and under Canada where wave path coverage is reduced [*van der Lee and Nolet*, 1997b]. Depth resolution is of the order of 50 km in the shallow mantle. Amplitudes of the velocity anomalies are well recovered in the upper 250 km but more damped in the lower part of the model [*van der Lee and Nolet*, 1997b].

[7] One *P* velocity model we use is the North American part of the global mantle velocity model named BSE-NL [*Bijwaard and Spakman*, 2000] (Figure 2b), which is an upgrade of model BSE98 [*Bijwaard et al.*, 1998], obtained with a nonlinear inversion technique that performs 3-D ray tracing after each iteration. The model is based on the reprocessed International Seismograph Centre (ISC) arrival time data set [*Engdahl et al.*, 1998] for the seismic phases *P*, *pP*, and *pwP*. Because of the use of a variable grid the model yields well-resolved regional velocity structure in areas of dense data coverage. In the western United States this model has a minimum horizontal resolution length of around 100 km. Vertical resolution is of the order of 50–100 km. In the shallow mantle the mostly vertically traveling rays result in some vertical smearing of velocity anomalies. Although shallow mantle velocities are well resolved under part of the eastern United States, resolution deteriorates under the stable craton due to lack of data (Figure 2b).

[8] The second V_P model is the western U.S. model that we will refer to as WUS00 [*Dueker et al.*, 2001; K. G. Dueker, personal communication, 2000]. This model amalgamates the various upper mantle *P* velocity models for the western United States of Dueker and coworkers [*Dueker et al.*, 1993; *Humphreys and Dueker*, 1994b; *Dueker*, 1999]. WUS00 is a regional model based on a large data set of teleseismic *P* and *PKIKP* travel times from several permanent and temporary arrays in the western United States. These arrays offer a dense data coverage for most of the western United States. A set of corrections for crustal structure using station statics, for Earth structure outside the region of interest using event statics and for timing differences between arrays using array statics, is applied. The resulting velocity model resolves features with horizontal dimensions as small as 50 km. Resolution varies laterally due to variable ray coverage. Vertical resolution is 50–100 km in the regions of better ray coverage. Because this regional model is based on locally corrected teleseismic data, it has little sensitivity to the regional background structure. The model extends down to 700 km, with the best resolution in the upper 400 km.

3. Inversion of Seismic Velocity for Temperature

[9] We invert seismic velocities for temperature using the procedure described by *Goes et al.* [2000]. This procedure is based on an infinitesimal strain approximation for the calculation of

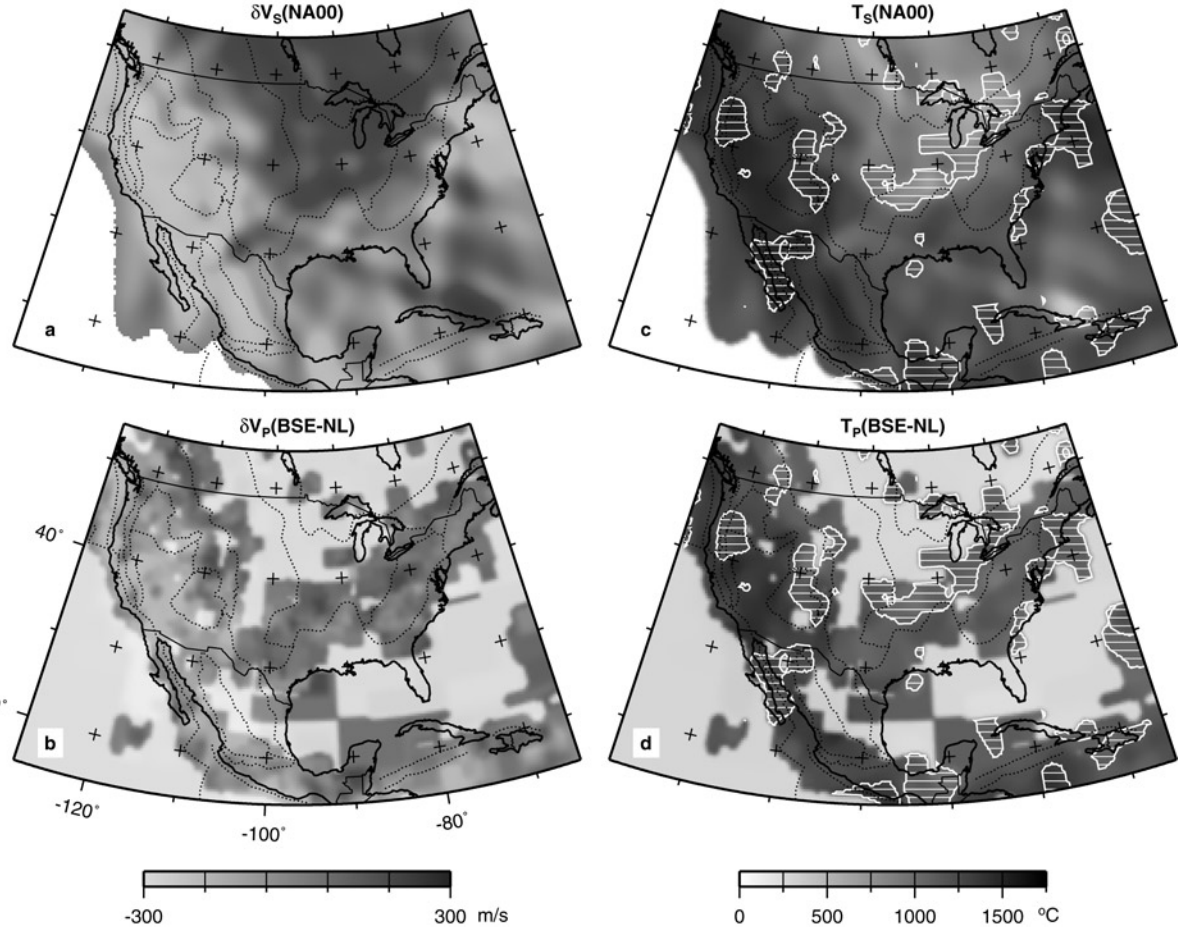

Figure 2. Maps of velocities and temperatures at 110 km depth. (a) Shear wave velocities from model NA00 [*van der Lee and Nolet*, 1997b] relative to a reference velocity of 4.5 km/s. (b) Compressional wave velocities from model BSE-NL [*Bijwaard and Spakman*, 2000] relative to reference model ak135 (8.05 km/s at this depth). Colors in Figures 2b and 2d are faded where the hit count of BSE-NL is below 200 and resolution deemed low. Velocity anomalies are shown in m/s. Note that on a percent scale, *S* velocity anomalies would be about twice as strong as *P* velocity anomalies. (c) Temperatures estimated from NA00. (d) Temperatures inferred from BSE-NL. Both thermal models were smoothed over a length scale of 300 km using a moving Gaussian window. Temperatures may be unreliable in the hatched regions where T_S and T_P differ by more than 150°C. The acgl composition and Q_1 anelasticity model were used for the interpretation of the seismic velocities. See color version of this figure at back of this issue.

seismic velocities for different temperatures, pressures, and compositions. The elastic constants and density and their dependence on *T*, *P*, and composition are taken from the mineral physics literature (see *Goes et al.* [2000] for the parameter values and references). The infinitesimal strain approximation significantly simplifies the calculation of velocity to temperature derivatives and is a reasonable approximation down to ~200–250 km depth.

[10] Important in evaluating the sensitivity of velocity to temperature is the inclusion of the nonlinear effect of anelasticity [*Karato*, 1993; *Sobolev et al.*, 1996]. At temperatures approaching the solidus, anelasticity may double the value of the partial derivative $\partial V/\partial T$, making it necessary to include this effect in evaluating low-velocity anomalies, although the experimental parameters describing anelasticity are less than optimally constrained [e.g., *Karato and Spetzler*, 1990]. Consistent with seismological observations we assume that attenuation is dominated by shear attenuation, Q_S. Bulk attenuation is taken to be 1000 or equal to Q_S when Q_S is higher than 1000. We use two different Q_S anelasticity models that span a range of the experimental results [*Goes et al.*, 2000]. Q_1 is a more average estimate of the temperature sensitivity of Q_S [*Sobolev et al.*, 1996] and Q_2, which is based on the experimental parameters for synthetic forsterite [*Berckhemer et al.*, 1982], represents a strongly temperature-dependent end-member. The parameters for Q_2 were measured near the solidus, but anelasticity does not appear to be affected by the presence of melt (at least at the low melt fractions expected in the mantle) [*Berckhemer et al.*, 1982; *Karato and Spetzler*, 1990].

[11] Forward calculations indicate that temperature is the main parameter affecting seismic velocities in the depth range 50–250 km [*Jordan*, 1979; *Nolet and Zielhuis*, 1994; *Sobolev et al.*, 1996; *Goes et al.*, 2000]. Therefore *P* and *S* wave velocities are inverted independently for mantle temperature. An iterative conversion similar to the procedure by *Sobolev et al.* [1996] is performed to take into account the temperature dependence of $\partial V/\partial T$. Because of this nonlinear dependence of velocity on temperature we cannot interpret velocity anomalies but invert absolute velocities for absolute temperatures. Uncertainties in the absolute temperature estimates based on uncertainties in the experimental parameters are estimated to be 100–200°C, but uncertainties in lateral variations in temperature are less [*Goes et al.*, 2000].

Table 1. Compositions

Name	ol/opx/cpx/gt, %	Mg #	Reference
Primitive garnet peridotite (pgp)	58/18/10/14	89	*McDonough* [1990]
Average continental garnet lherzolite (acgl)	67/23/4.5/5.5	90	*Jordan* [1979]
Archaen subcontinental lithosphere (arch)	69/25/2/4	93	*Griffin et al.* [1999]

[12] Although temperature is the dominant effect, we perform inversions with different mantle compositions to illustrate this effect. The three compositions we used are summarized in Table 1. They represent a nondepleted mantle composition, primitive garnet peridotite (pgp) [*McDonough*, 1990], a somewhat depleted composition which *Jordan* [1979] defined as an average continental garnet lherzolite composition for the lithosphere (acgl) and a strongly depleted composition (arch) inferred from xenoliths from Archean cratons [*Griffin et al.*, 1999]. The experimental parameters used are listed and discussed in more detail by *Goes et al.* [2000]. Composition is an important factor for seismic velocities in the crust. However, none of the tomographic models that we use has good resolution for crustal structure, and we interpret only mantle seismic velocities.

[13] Where temperatures above the solidus are found, the effect of melt has to be considered. The presence of melt and other fluids (e.g., water) lowers both V_P and V_S but the effect on V_S is stronger than the effect on V_P [*Schmeling*, 1985; *Hammond and Humphreys*, 2000]. If such fluid-affected velocities are interpreted in terms of temperatures, the temperatures obtained from V_S will exceed those obtained from V_P since the relative sensitivity to temperature of V_S and V_P, ($\partial \ln V_S/\partial \ln V_P$) is less than the relative sensitivity to the presence of fluids. The effect of melt can vary between ~0.5 and 14.5% velocity decrease per percent melt depending on the geometry of the melt pockets and on whether they are connected or not [*Schmeling*, 1985; *Hammond and Humphreys*, 2000].

[14] The presence of water may affect the velocities even at temperatures below the solidus, be it as free water, or in hydrated minerals which generally have a significantly lower velocity than average mantle minerals [*Sobolev and Babeyko*, 1994; *Bass*, 1995]. Anelasticity, since it appears to be creep related [*Karato and Spetzler*, 1990] probably depends on temperature relative to the melting temperature in a similar manner as rheology does. Therefore the presence of water which lowers the melting temperature will decrease Q_S and increase $\partial V/\partial T$ [*Karato and Jung*, 1998].

[15] Finally, the presence of seismic anisotropy may bias our temperature estimates that are based on the assumption that the velocities mapped are average isotropic values. Anisotropy will bias isotropic velocity estimates in areas where seismic sampling is dominated by one propagation or polarization direction. *Sobolev et al.* [1999] studied the bias that anisotropy may have on isotropic velocity estimates from teleseismic *P* wave tomography. They suggest that while thermal and compositional effects on velocities should have correlated effects on *P* and *S* velocities, anisotropy would have disparate effects. The use of both V_P and V_S may thus allow for the identification of anisotropy. V_P estimates used here are based on predominantly vertically propagating *P* waves and the V_S estimates are based on horizontally propagating Rayleigh waves from many different azimuths.

4. Comparison of Temperature Estimates

[16] We first discuss uncertainties in the temperature estimates and compare the temperatures inferred from V_P (from BSE-NL) and V_S (from NA00) with each other and with temperatures in the conductive lithosphere as obtained from surface heat flow. The interpretation of the mantle temperatures and comparison with the smaller-scale velocity model WUS00 is discussed in section 5.

4.1. Effect of Composition and Anelasticity

[17] Figure 3 shows our average geotherms for the eastern region encompassing the Midcontinent, the Superior and the Grenville provinces, and the western region comprising the Columbia Plateau/Snake River Plain, the Basin and Range and the Colorado Plateau. For reference, Figure 3 shows a mantle adiabat with a 1300°C surface temperature which is thought to be a reasonable estimate of temperature of the asthenosphere [*McKenzie and Bickle*, 1988], as well as the wet and dry peridotite solidi [*Thompson*, 1992]. A geotherm estimated from V_P is only shown for the western United States since resolution is poor in much of the region comprised in the eastern U.S. average. These average geotherms show a difference of ~500°C at the shallowest depths between the western and eastern part of the continent. The difference in temperature persists down to ~200–250 km depth.

[18] Curves 1 and 2 illustrate the effect of two different compositional models. Curve 1 was calculated using a primitive mantle composition (pgp, Table 1) and gives the lowest temperature estimates, curve 2 was calculated with a strongly depleted composition (arch) and gives the highest temperatures. The shaded

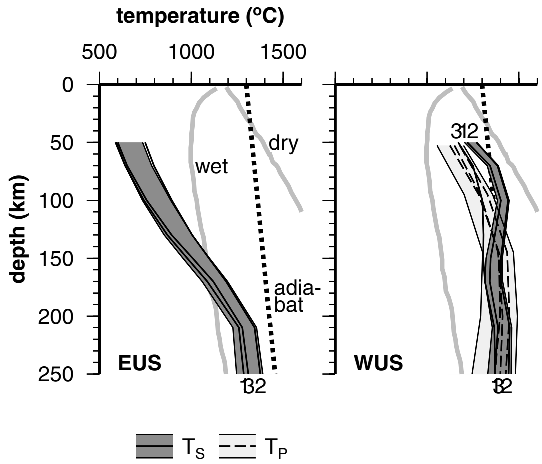

Figure 3. Average geotherms for eastern (Midcontinent, Canadian Shield, and Grenville Provinces, Figure 1) and western (Basin and Range, Columbia, and Colorado Plateaus) North America. Temperatures inferred from the *S* wave velocities of NA00 (T_S, solid lines with dark shaded uncertainty range based on uncertainties in the experimental parameters) and (for western North America only) temperatures inferred from V_P of BSE-NL (T_P, dashed lines with light uncertainty range) are shown for depths larger than 50 km. The gray lines show the positions of the wet and dry peridotite solidi [*Thompson*, 1992], the bold dotted line is a mantle adiabat with a potential temperature of 1300°C. Three different seismic geotherms are shown: curve 1, using a primitive peridotite composition (pgp, Table 1) and average anelasticity model Q_1 [*Sobolev et al.*, 1996]; curve 2, using a strongly depleted peridotite composition (arch, Table 1) and average anelasticity model (Q_1); and curve 3, using a primitive garnet peridotite composition (pgp) and strongly temperature-dependent anelasticity model Q_2 [*Berckhemer et al.*, 1982]. The shaded region illustrates the uncertainty in temperatures estimated with a more average continental peridotite composition (acgl, Table 1) and Q_1. The effect of composition falls completely within this uncertainty range. The anelasticity model only affects the highest-temperature estimates.

region shows the uncertainty range of temperatures calculated using the average somewhat depleted composition (acgl), which we use in the remainder of this paper unless noted otherwise. The uncertainties are based on uncertainties in the mineralogical parameters used in the inversion from velocities to temperature [*Goes et al.*, 2000]. There is an influence of composition on the estimated temperature and this effect is largest in the cold regions where anelasticity plays a small role. However, the resulting temperatures differ by only 100–200°C and all fall within the uncertainty range of the temperature estimated with the acgl composition. Compositional models pgp and arch span the range of plausible average mantle compositions. Other mantle rocks such as hydrated phlogopite peridotites or eclogites have stronger seismic signatures but are unlikely to determine velocities averaged over 100–200 km length scales. The transition from spinel to garnet peridotite which occurs within a 60–80 km depth range will also have a small effect on the seismic velocities, but this falls within the range that is spanned by the compositional models used in Figure 3 [*Goes et al.*, 2000]. The presence of plagioclase peridotite would have a stronger effect, but it transforms to spinel peridotite at ~30 km depth.

[19] Curves 1 and 2 in Figure 3 have been computed using anelasticity model Q_1. Curve 3 is for the same composition as curve 1 (pgp) but for anelasticity model Q_2, which has a relatively extreme dependence on temperature. Although the parameters for anelasticity are much less well constrained than those of the elastic parameters and density, we think the difference between models Q_1 and Q_2 gives a reasonable assessment of the uncertainty that the anelasticity model introduces in the temperature estimates [*Goes et al.*, 2000]. Using Q_2 has a negligible effect on the temperature under the relatively cool eastern United States but affects the estimates of temperatures that are within a factor of 0.8–0.9 of the mantle solidus, such as under the Basin and Range. It can be seen (Figure 3) that differences between T_P and T_S under the western United States fall completely within the uncertainty range of the anelasticity models.

4.2. Comparison of T_P and T_S

[20] Temperatures at 110 km depth inferred from V_P (from BSE-NL) and V_S (from NA00) are shown in Figures 2c and 2d. Comparing the temperatures from these two velocity models is not straightforward. First, the *P* velocity model resolves smaller-wave-length features than the *S* velocity model (Figures 2a and 2b). To make a visual comparison easier, we have smoothed both T_P and T_S in Figure 2 with a moving Gaussian window with a diameter of 300 km. Second, the *P* velocity model BSE-NL does not have much resolution in the Midcontinent and thus does not show the strong contrast between the western and eastern United States which is the first-order feature in the *S* velocity model NA00.

[21] To quantitatively compare the two temperature models, we averaged temperatures from V_P and V_S (unsmoothed) within circles of a radius of 100 km (Figure 4) and compare averaged T_P and T_S (Figure 5). The circles were distributed so as to capture the main resolved features of the two velocity models. The circle radius of 100 km is a compromise between the scale of the well-resolved anomalies and the scales that can be resolved by the different tomographic inversions. T_P from BSE-NL and T_S from NA00 agree within 150°C for two thirds of the regions at 50 km depth, for three quarters of the regions at 100 km and for all the regions below 100 km depth (Figure 5).

[22] At 50 km depth, part of the scatter may be due to remaining trade-off between mantle velocities near the Moho and crustal structure. The differences in Moho depth between NA00 and NA95 are up to 10 km. Temperatures calculated from the two models show that at a comparable data fit, a 10-km change in Moho depth results in a change in temperature estimate of up to 300°C at 50–70 km; that is, the effect is certainly large enough to account for the scatter. Below 70 km depth, V_S and T_S are hardly

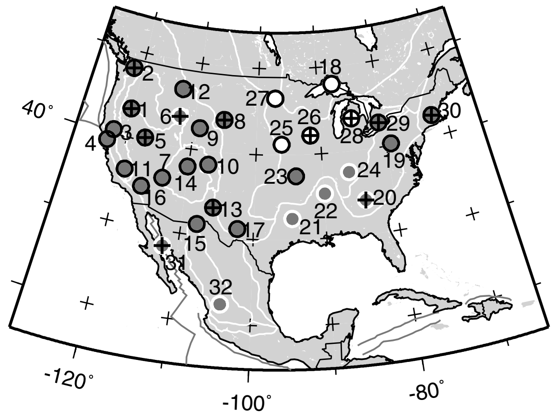

Figure 4. Map showing the locations of averaged geotherms discussed in the text. In addition to geotherms from V_S, shaded circles have geotherms from V_P, and circles with solid rims have geotherms estimated from surface heat flow (T_q). All geotherms with both T_S and T_P estimates are used for the comparison in Figure 5, all geotherms with T_q estimates are used for the comparison in Figure 6. A selection of geotherms (circles with plusses) is shown in Figure 7.

affected by trade-off with Moho depth. V_P in the shallowest mantle layer (centered around 50 km depth) may also be affected by unmodeled crustal structure.

[23] Most of the regions where T_P and T_S disagree at 50 km are, however, the same as those where T_P and T_S disagree at 100 km, suggesting a noncrustal origin. Narrow high-velocity anomalies, e.g., under Oregon/Washington (circle 2) and under California (circle 3) cause discrepancies since they are not well resolved in NA00. This is due to (1) their relatively small scale and (2) the higher sensitivity of spatially averaged V_S to nearby lower-velocity regions, which is the result of the nonlinear dependence of $\partial V/\partial T$ on *T*. Spatially averaged velocities are an underestimate of the velocity corresponding to the averaged temperature, and this effect is stronger for V_S than for V_P. Figures 2c and 2d, where the smoothing window has removed small-scale features, show where larger-scale differences between T_P and T_S exist and temperature estimates may be incorrect. Four regions with significant T_P–T_S discrepancies are identified: overlying the Cascadia slab (including circle 2), below the Gulf of California, under the northern Colorado Plateau and Wyoming (including circles 14, 9, and 8) and at the border of the Midcontinent region. Resolution tests show that the amplitudes of the V_P velocities in this region tend to be more underestimated than elsewhere (W. Spakman, personal communication, 2000). Therefore much of the T_S–T_P discrepancy under the Midcontinent is probably due to insufficient resolution.

[24] Thus NA00 and BSE-NL give temperatures that agree within their uncertainties where both models have good resolution, with the exception of the Cascadia mantle wedge, the mantle at 50–100 km depth under the Gulf of California and the shallow mantle under Wyoming. In these regions, temperature is probably not the only factor influencing seismic velocities.

4.3. Comparison With Temperatures From Surface Heat Flow

[25] Surface heat flow measurements have shaped the general view of the thermal structure of the conductive lithosphere. Here we compare our seismic temperature estimates with the independent temperature estimates obtained from surface heat flow.

[26] *Artemieva and Mooney* [2001] published global maps of temperature at 50, 100, and 150 km depth. In the eastern part of North America their temperatures are from steady state geothermal

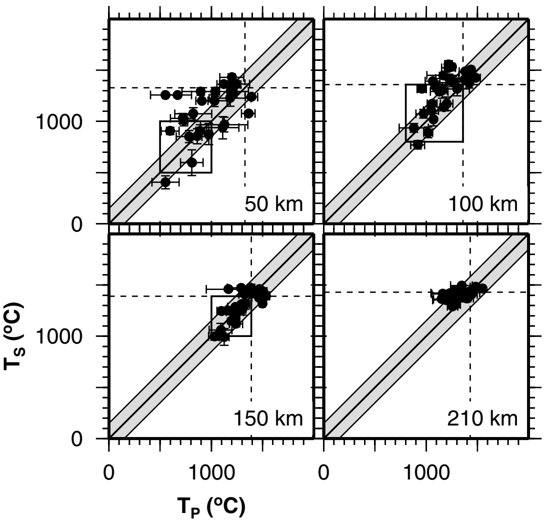

Figure 5. Comparison of the temperatures inferred from NA00 (T_S) and from BSE-NL (T_P) averaged over the shaded circles in Figure 4. The comparison is shown for several depths. If agreement would be perfect, the points should fall on the $T_S = T_P$ line (thick solid line). For about two thirds of the regions, T_S and T_P agree within 150°C (shaded region). Discrepancies can partly be explained by differences in spatial resolution between the two tomographic models but may also indicate that other effects than temperature affect the seismic velocities. Error bars illustrate the variation in temperature within the circles. Temperature estimates are for the composition acgl (Table 1) and the anelasticity model Q_1. The range of temperatures at 50, 100, and 150 km depth estimated by *Artemieva and Mooney* [2001] from North American surface heat flow is outlined by the square, and the temperature that a 1300°C mantle adiabat reaches at each depth is marked by the dashed lines.

modeling of reevaluated heat flow and heat production data. In the western United States their temperatures are from previously published petrological and nonsteady state geotherms. The lower bound of the temperatures of *Artemieva and Mooney* [2001] (Figure 5) agrees well with the lower bound of our seismic temperatures at all three depths. At 100 and 150 km depth the highest temperatures of *Artemieva and Mooney* [2001] follow a mantle adiabat, in agreement with the seismic temperatures which are, within their uncertainties, also bounded by a 1300°C mantle adiabat. At 50 km depth the maximum temperature of *Artemieva and Mooney* [2001] is ~1000°C, while the seismic temperatures under parts of the western United States reach the mantle adiabat. The high shallow seismic temperatures are, however, consistent with regional heat flow analyses that attribute high heat flow values in the Basin and Range [*Lachenbruch et al.*, 1994] and in some parts of the southern Rocky Mountains/Rio Grande region [*Decker*, 1995] to high temperatures at the base of the crust. There is a strong lateral variation and under other parts of the western United States (e.g., Colorado Plateau and other parts of the southern Rocky Mountains) geothermal modeling has yielded temperatures below 1000°C at 50 km depth [*Decker*, 1995; *Artemieva*, 1996].

[27] For a point-by-point comparison similar to that done for T_P and T_S we determined temperatures at depth from the global heat flow database [*Pollack et al.*, 1993]. Heat flow values were averaged over the same 100 km radius circles of Figure 4. We use *Chapman*'s [1986] family of steady state conductive geotherms which are based on the assumption that crustal heat production is responsible for 40% of the surface heat flow [*Pollack and Chapman*, 1977]. Below the conductive lithosphere, heat flow derived temperatures are assumed to follow a 1300°C mantle adiabat. The smoothing of the surface heat flow over the circles in Figure 4 somewhat reduces local effects of ignored subsurface advection and lateral variations in heat production. In addition, we assign a relatively large uncertainty of ±20% to the surface heat flow to encompass the effect that the uncertainties in the various thermal parameters [*Chapman*, 1986] have on the geotherms. We exclude circles 6, 20, and 22, where low heat flow values are known to be associated with shallow fluid flow [e.g., *Morgan and Gosnold*, 1989]. For circles 21, 24, 31, and 32, there are no heat flow data.

[28] The correlation is shown in Figure 6 for temperatures at 50 km depth. Our heat flow temperature estimates give adiabatic temperatures at 50 km depth in several parts of the western United States. Although the assumption of a steady state thermal state is debatable for many of these regions, nonsteady state models [*Lachenbruch et al.*, 1994; *Decker*, 1995] give similarly high temperatures at 50 km depth. There is more scatter in $T_{P,\,S}$ versus T_q than in the correlation between T_P and T_S at 50 km depth (Figure 5). Influence of crustal structure on subcrustal seismic velocities and improperly modeled crustal contributions to surface heat flow may play a role in the scatter, as discussed above. However, for the correlation between T_P and T_q only 20% of the points fall outside a range of ±200°C. Three of these points lie in California (circles 3, 4, and 11), where stronger lateral variations are seen in the heat flow than can be resolved in BSE-NL or NA00. The more detailed model WUS00 does show lateral variations in seismic velocity that correlate well with those in surface heat flow [*Humphreys and Dueker*, 1994a]. The only other significant outlier is a point in the northern Rockies (circle 12), where heat flow values are locally high. This may be a local effect of crustal properties as documented for the southern Rockies [*Decker*, 1995]. The correlation plot of T_S and T_q has more outliers, ~40% of all points. Half of these outliers are for the same points where T_P and T_q disagree, and T_S and T_q probably disagree for the same reasons. Almost all of the other points are points where T_P and T_S also disagree at 50 km. These are discussed in detail in section 4.2. The agreement between T_P and T_q for the points where T_P and T_S

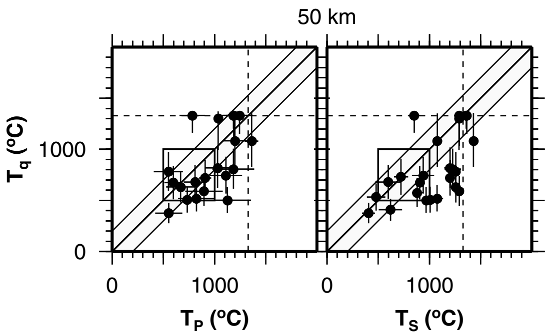

Figure 6. Comparison of temperatures estimated from surface heat flow and from seismic velocities. Temperatures at 50 km estimated from surface heat flow (T_q) by extrapolating down along steady state geotherms against temperatures from seismic velocities (T_P from BSE-NL and T_S from NA00 using acgl and Q_1). Surface heat flow data are from the Global Heat Flow database [*Pollack et al.*, 1993]. Error bars for seismic temperatures illustrate the variation within the circles shown in Figure 4. Error bars for T_q reflect the effect of a ±20% uncertainty in average surface heat flow. As in Figure 5, the square outlines the range of temperatures at 50 km depth estimated from North American surface heat flow by *Artemieva and Mooney* [2001], and the dashed lines mark the temperature at 50 km depth of a 1300°C mantle adiabat. Agreement of the temperature estimates within 200°C (thin lines) is considered reasonable. If agreement would be perfect the points should fall on the $T_q = T_{P,\,S}$ line (thick solid line).

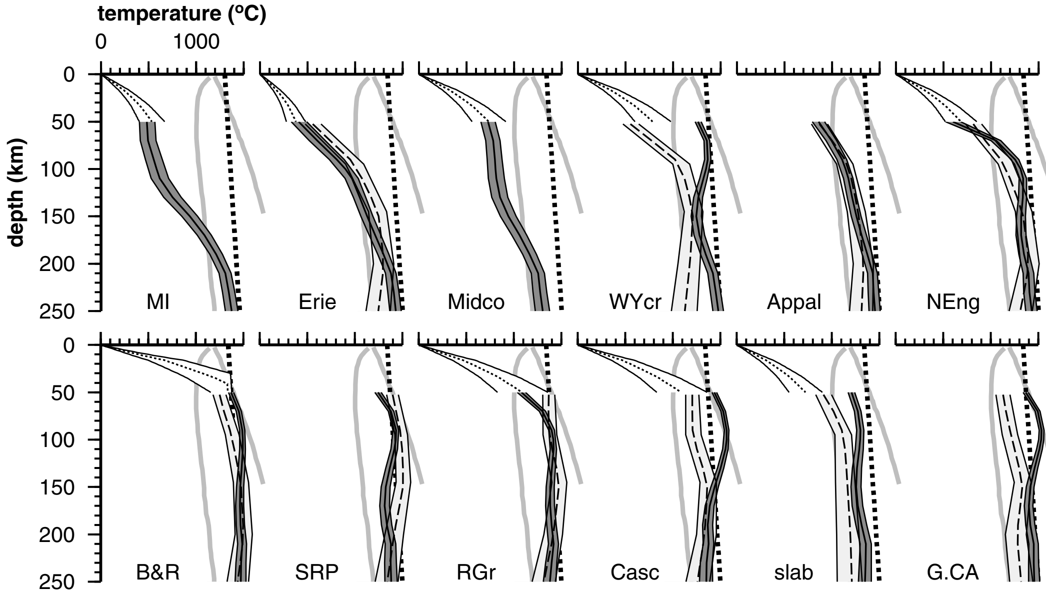

Figure 7. A selection of geotherms averaged over the circles with plusses shown in Figure 4. Lines and shading are as in Figure 3. Velocity-derived geotherms with uncertainty ranges for the acgl composition and Q_1 anelasticity are shown. Temperatures from heat flow are displayed as dotted lines with a white range based on a 20% uncertainty in surface heat flow. (top) Geotherms from the region east of the Rocky Mountain Front for locations in the Midcontinent in Michigan (circle 28), under Lake Erie (circle 29), and east of Lake Michigan (circle 26), in the Wyoming craton (circle 8), in the southern Appalachians (circle 20), and in New England (circle 30). (bottom) Geotherms from western North America for the northern Basin and Range (circle 5), the eastern Snake River Plain (circle 6), the northern part of the Rio Grande Rift (circle 13), the Cascades anomaly (circle 2), the Cascadia slab under Washington (circle 1), and the Gulf of California (circle 31).

disagree indicates that T_P provides a reasonable estimate of mantle temperature for these regions. At a few points in the Midcontinent, T_q and T_S could be compared where no T_P is available. The temperatures agree for these points with the exception of Lake Superior (circle 18). This region has a highly anomalous crust with a large thickness, very low heat production, and high seismic velocities [e.g., *Braile et al.*, 1989; *Morgan and Gosnold*, 1989; *Chulick and Mooney*, 1998], and therefore T_S and T_q may both be incorrect. The agreement of T_S in the Midcontinent with our T_q and with the temperatures determined by *Artemieva and Mooney* [2001] substantiates that the T_S–T_P discrepancy under the Midcontinent (Figure 2, section 4.2) is mostly due to insufficient resolution of the V_P anomalies.

[29] Overall, we deem the agreement between temperatures from surface heat flow and temperatures from seismic velocities to be good, given the uncertainties. Especially, the range in temperatures from velocities and heat flow agrees well. This confirms our initial assumption that seismic velocities in the shallow mantle predominantly reflect variations in temperature.

5. Thermal Structure

[30] For the interpretation of the thermal structure in section 5.1 we concentrate on the structure on a length scale that is well resolved in both NA00 and BSE-NL (i.e., >200–300 km). In section 5.2, comparison with the smaller-scale model WUS00 allows a more detailed discussion of the mantle structure under western United States.

5.1. Continental-Scale Shallow Mantle Temperatures

[31] The large-scale thermal structure (Figure 2) is discussed by tectonic region. Selected geotherms from the comparison of T_P, T_S, and T_q are shown in Figure 7. For locations we refer to Figures 1 and 4.

5.1.1. Midcontinent/craton. [32] Significant variations in eastern North American lithospheric temperature are predicted by *P* and *S* wave velocities and by surface heat flow data. *Morgan and Gosnold* [1989] attribute variability in eastern U.S. heat flow (east of the Rocky Mountain front) mainly to crustal structure and shallow groundwater flow and treat the whole eastern part of the continent as one thermal province. However, V_S and V_P indicate that differences in deeper thermal structure do exist. First, there is a difference of ∼200–300°C between the region below the North American craton and the off-cratonic regions of the Appalachians, coastal plains, and western part of the Great Plains (Figure 2), even if a difference in composition between the cratonic (more depleted) and off-craton regions (less depleted) is assumed. Second, there appears to be a variability of several hundred degrees within the North American craton (Figures 2c and 7 (top)). For example, at 50 km depth, temperatures vary between 500 and 900°C. Since the last tectonic activity in the interior eastern United States dates back to ∼1 Ga, the modeled variations in temperature cannot be thermotectonic in origin, as they would have diffused over timescales of tens to a few hundreds of millions of years. The inferred differences in thermal structure could be the result of variations in lithospheric thickness and coupled to the lateral variations in thickness of the conductive thermal boundary layer. These lithospheric thickness undulations would have to be a relict of Precambrian tectonics and could be preserved due to a buoyant lithospheric composition [*Jordan*, 1979] and/or high lithospheric viscosity resulting from the extraction of water [*Hirth and Kohlstedt*, 1996]. For example, some higher temperatures at the western boundary of the Midcontinental region correlate with the position of the Midcontinent Rift, where the lithosphere may be thinned compared to the more stable continent to the east.

[33] The lithosphere under the Wyoming craton has a low shear velocity anomaly where V_P is high (Figure 2). This disagreement between T_P and T_S (Figure 7) is difficult to explain. *van der Lee and Nolet* [1997b] suggest that the low V_S is a manifestation of the craton's anomalous character that has been attributed to extensive metasomatism [*Carlson et al.*, 1999]. Metasomatism can produce low-velocity hydrated minerals but would lower both V_P and V_S [*Sobolev and Babeyko*, 1994; *Bass*, 1995]. Furthermore, the hydrated minerals would need to be present in large enough quantities to produce seismic anomalies on a 100-km scale. Seismic anisotropy might be an alternative explanation, but there is no lattice preferred orientation that would both increase V_P from teleseismic body waves and decrease V_S from azimuthally averaged Rayleigh waves.

5.1.2. Off-craton eastern United States. [34] Generally, V_P and V_S yield consistent temperature estimates here (Figure 2), including some higher temperatures under the southern Appalachians (circle 20, Figure 7) and beneath the Gulf Coast (circle 22). Many of the surface heat flow measurements in the southeastern United States give very low values (10–30 mW/m^2), but this has been interpreted to reflect shallow fluid flow rather than deep temperatures [*Morgan and Gosnold*, 1989]. This interpretation is corroborated by the not exceptionally low seismic temperatures under this region. The seismic temperatures are 700–1000°C at 50 km depth (e.g., Figure 7, curve for the Appalachians), very consistent with the temperatures of 700–800°C that *Artemieva and Mooney* [2001] estimated at this depth.

[35] NA00 implies high temperatures in places along the East Coast, specifically under New England (circle 30). At 50 km depth, surface heat flow, V_P, and V_S provide similar temperature estimates that are not unusually high for the eastern part of the continent (600–700°C, Figure 7). By 100-km depth, however, T_S has risen to around 1200°C. There is some indication of higher T_P along the East Coast as well, but not as high as T_S (Figure 2). The difference between T_S and T_P could be produced by hydration of the deep lithosphere, as suggested by *van der Lee and Nolet* [1997b].

5.1.3. Basin and Range, Columbia, and Colorado Plateau. [36] A large-scale low-velocity anomaly that extends down to 350–400 km depth is found under Nevada in both NA00 and BSE-NL. Temperatures estimated for the Basin and Range follow the 1300°C adiabat up to depths as shallow as 50 km (Figure 7), indicating shallow asthenosphere and very thin lithosphere for this region. These shallow high temperatures extend under the Snake River Plain (Figures 2 and 7), around the Colorado Plateau and under its southwestern edge, under the Rio Grande Rift area, and under parts of the southern Rocky Mountains (Figure 2). V_S gives slightly higher temperature estimates than V_P and T_S has a negative gradient around 100 km depth (Figures 3 and 7). Higher T_S than T_P within a depth range of 50–100 km is the type of signature expected if melt is present. However, the sensitivity to the Q_S model (Figure 3) shows that the difference in T_P and T_S and the negative gradient in T_S fall within the uncertainties. Since there is no resolvable disagreement between T_P and T_S, there is no indication for the presence of melt on a large scale under the western United States as proposed by *Humphreys and Dueker* [1994a]. However, temperatures are high enough that a small increase in temperature or the addition of some water could lead to melting and the presence of small-scale melt pockets (smaller than the 100–200 km scale resolved in BSE-NL and NA00) is likely.

[37] Low shear wave velocities continue under most of the Colorado Plateau, although the anomalies vary in amplitude (Figure 2a). BSE-NL, however, maps high *P* wave velocities in the central and northern part of the plateau (Figure 2b) which translate to temperatures as low as 800–1000°C at 50 km depth. We obtain even lower temperatures (400–700°C) in the shallow lithosphere of the Colorado Plateau from steady state modeling of surface heat flow. However, the surface heat flow values on the plateau have been interpreted to be transient and to reflect a previous cooler state of the mantle [*Morgan and Gosnold*, 1989]. T_P and T_S are consistent below 150 km (Figure 5). The difference between T_P and T_S at shallow depths (Figure 2) is probably at least partly due to the fact that NA00 has not resolved the sharp lateral gradients within the plateau mapped by *P* waves. However, the Colorado T_S–T_P anomaly merges with that associated with the Wyoming low V_S anomaly (Figures 2c and 2d), and it cannot be precluded that the seismic signature of the lithosphere under the Colorado Plateau (and parts of the Rocky Mountains) has been modified in a similar way as the lithosphere under Wyoming.

5.1.4. U.S. West Coast. [38] The lowest *S* velocity anomaly in NA00 (Figure 2a) is located between 50 and 100 km depth more or less under the Cascades (circle 2 in Figure 4). When interpreted in terms of temperature this low V_S gives temperatures that exceed the dry solidus (Figure 7). Although some low *P* velocities are mapped in this region as well (Figure 2b), these do not translate into anomalously high temperatures (Figures 2 and 7). Nor is the surface heat flow consistent with high mantle temperatures (Figure 7) (except locally in volcanic regions). In Japan [*Iwamori and Zhao*, 2000], Tonga [*Koper et al.*, 1999], and South America [*van der Lee et al.*, 2001], extremely low velocity in the mantle wedge has been attributed to water released from the subducting oceanic plate. It seems likely that much of the low V_S anomaly above the Cascadia slab is also attributable to the presence of fluids. The expelled slab fluids will allow the formation of the melt that feeds the Cascade volcanoes, at relatively low mantle temperatures of 1100–1200°C.

[39] Both velocity models show the horizontal gradient from lower temperatures (700–1100°C between 50 and 100 km depth) along the California coast up to the Mendocino Triple Junction (at 40°N) to asthenospheric temperatures under eastern California (Figure 2), and both models show asthenospheric temperatures north of the Mendocino Triple Junction along the coast of Oregon and Washington. More detailed structure is not well resolved in NA00 and is discussed further in section 5.2.

5.1.5. Mexico. [40] The Gulf of California is characterized by low *S* wave velocities, which translate into superadiabatic temperatures between 50 and 150 km and adiabatic mantle temperatures below 150 km depth. The bulge in T_S near 80 km may well be an expression of the presence of melt, as would be expected in this depth range under a spreading ridge. *P* velocities do not yield similarly high temperatures (Figure 2). However, resolution of V_P may not be sufficient since the Gulf of California lies on the edge of the well-resolved region of BSE-NL, and the *P* velocities under the gulf are close to the background model (Figure 2b). The very high T_S makes a contribution from the presence of partial melt to the seismic velocities likely and a positive T_S–T_P anomaly is consistent with this interpretation.

[41] Under the southern part of the Rio Grande Rift (circle 15), T_S reaches the dry solidus at the shallowest depths, T_S has a negative gradient between 100 and 150 km, and T_P and T_S are significantly different. This signature is the same as that of the Cascadia and Gulf of California anomalies, and we consider it likely that here too the velocities are affected by the presence of partial melt, consistent with recent extension and volcanism here. Farther north along the rift, the lateral extent of melt present may be too small to have an expression in the long-wavelength velocity models.

[42] The Sierra Madre Occidental in Mexico is underlain by low *P* and *S* velocities, which extend south to about 20°N, the latitude of the Trans-Mexican volcanic belt. The low velocities may extend east and west of the Sierra Madre Occidental, but the lateral extent is not conclusively resolved in either NA00 or BSE-NL. The Sierra Madre Occidental is a relatively undeformed but elevated block within the southern extension of the U.S. Basin and Range Province [*Henry and Aranda-Gómez*, 1992]. North of the Trans-Mexican volcanic belt, subduction has ceased, and extension

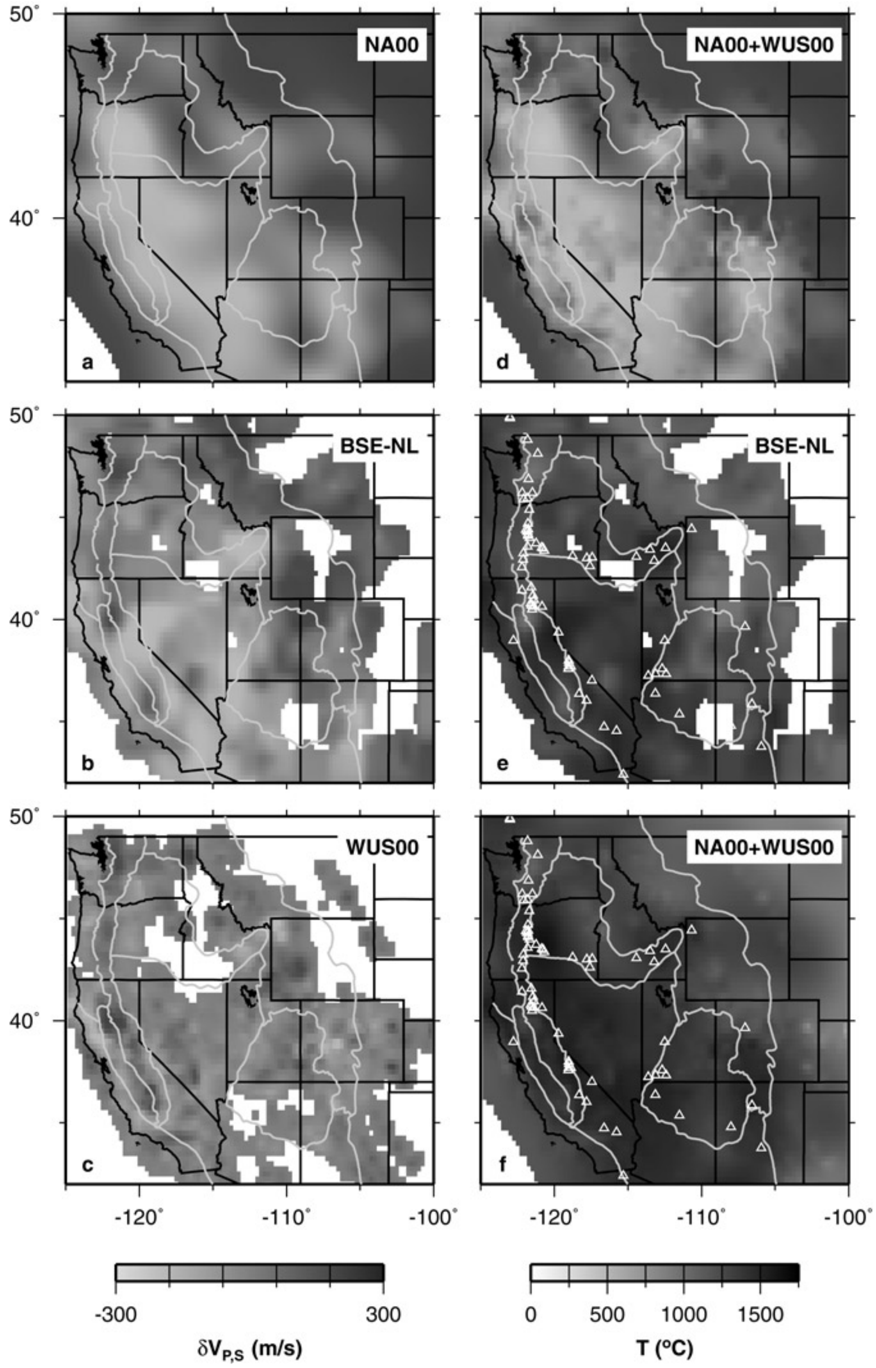

Figure 8. Maps at 110 km depth for the western United States for the three velocity models NA00 (V_S), BSE-NL (V_P), WUS00 (V_P) and a composite model of NA00 and WUS00 (V_S) and temperatures inferred from the composite V_S model and BSE-NL for the acgl composition and Q_1 anelasticity model. Velocity anomalies are shown in m/s relative to the average velocity in this region ($V_P = 4.29$ km/s, $V_S = 7.99$ km/s). Areas where no velocities are resolved are left white. Gray lines mark physiographic boundaries, black lines state boundaries (courtesy of K. Dueker). Yellow triangles show the location of Holocene volcanoes [*Simkin and Siebert*, 1994]. See color version of this figure at back of this issue.

similar to that in the U.S. Basin and Range has been ongoing since ~30 Ma. The temperatures that we find under the Sierra Madre are similar to those under the Basin and Range farther north; that is, they follow a mantle adiabat between 50 and 250 km depth. Thus the temperatures are consistent with the interpretation of tectonic continuity of the extension north and south of the U.S.-Mexico border. South of about 20°N active subduction is ongoing and seismic velocities are higher (Figure 2) than under northern Mexico.

5.2. Smaller-Scale Mantle Structure Under the Western United States

[43] Some surface tectonics do not have any expression in the long-wavelength velocity anomalies. For example, neither NA00

nor BSE-NL shows a distinct anomaly under Yellowstone, although low velocities under the eastern Snake River Plain are mapped (Figure 2). The subducting Juan de Fuca slab off the coast of Washington is imaged in BSE-NL, but it contributes only a minor anomaly to NA00 for reasons discussed in section 4.2. The model WUS00 fills these voids since it is based on data from dense networks allowing resolution of small-scale lateral variations in velocity. WUS00 is a model of velocity anomalies and needs to first be converted into absolute velocities to enable interpretation in terms of temperature. Subsequently, we comment on the main features of smaller-scale thermal structure under the western United States.

5.2.1. Thermal interpretation of WUS00. [44] WUS00 is a velocity anomaly model relative to a regional background. The background model chosen must reflect the relatively slow western North American regional velocity structure. Figure 8 shows velocity anomalies from BSE-NL and NA00 relative to a average one-dimensional (1-D) western U.S. reference model to make visual comparison with WUS00 velocity anomalies easier. It is clear from Figure 8 that the wavelengths of the velocity anomalies decrease from NA00 to BSE-NL and further to WUS00. NA00 includes only larger-scale features (dimensions >200–300 km), WUS00 shows only smaller-scale features (dimensions <100–200 km), and BSE-NL shows elements of both the other models. Tests that we performed show that the small-scale features seen in WUS00 are too small to be resolved by the waves used for constructing NA00; that is, they fall within the null-space of model NA00. On the basis of the lack of large-scale trends in WUS00 we presume the opposite is also true; that is, that the long-wavelength features from NA00 fall in the null-space of WUS00. This validates the approach of *Dueker* [1999], who superimposed an earlier version of WUS00 on the long-wavelength V_S model of *Grand* [1994] to provide an image of structure at all scales. We construct an updated composite model by superposition of WUS00 anomalies on NA00, after converting δV_P to δV_S, using $\delta V_S/\delta V_P$ calculated from the NA00 temperature field (Figure 8). The composite NA00 + WUS00 model is inverted for temperature and allows for a better comparison with temperatures from BSE-NL. Using a different background model for WUS00 will affect the estimates of absolute temperature more than of lateral temperature differences. At the high-temperature end (temperatures of $0.8–0.9T_{\mathrm{solidus}}$) the estimates of temperature differences are affected as well due to the nonlinear dependence of velocity on temperature.

5.2.2. Yellowstone/Snake River Plain. [45] WUS00 includes a strong low-velocity anomaly centered under the Yellowstone Caldera (Figure 8), which seems consistent with its extreme volcanic activity that has been attributed to the presence of a deep-seated mantle plume. Temperatures inferred from NA00 + WUS00 exceed the dry solidus around 50 km depth. BSE-NL and NA00 do not show the small-scale Yellowstone anomaly but do map temperatures which at 50 km depth approach the dry solidus under the eastern Snake River Plain (Figure 7), where WUS00 has low-velocity anomalies as well (Figure 8). Except for the local above solidus temperatures predicted by NA00 + WUS00 under Yellowstone, the temperatures under the region are similar to those under the Basin and Range and do not exceed an average mantle adiabat within our uncertainties. Limited resolution hampers imaging of a possible deeper plume structure under Yellowstone. In both BSE-NL and NA00 + WUS00 the anomaly under the Snake River Plain is a significant low-velocity anomaly down to ~250–300 km depth.

5.2.3. Basin and Range. [46] WUS00 has a high-velocity anomaly in central Nevada, where lower surface heat flow and higher velocities in BSE-NL are also observed (Figure 8). This high-velocity anomaly is strong enough to give a signature in the composite NA00 + WUS00 model and translates into temperatures that are 100–200°C lower than the surroundings (Figure 8). WUS00 also resolves small-scale low velocities which correlate well with the locations of recent volcanism along the edges of the Basin and Range (Figure 8) [*Humphreys and Dueker*, 1994a]. In the composite model NA00 + WUS00 several of these anomalies give temperatures that exceed the dry solidus in the 50–100 km depth range. This indeed lends credence to the presence of small-scale melt pockets, for example, along the western edge of the Colorado Plateau and in the northern part of the Rio Grande Rift.

5.2.4. West Coast anomalies. [47] The Juan de Fuca slab under Washington has a clear expression in both the composite model NA00 + WUS00 and in BSE-NL, and both models give consistent slab temperatures (Figure 8). At 50 km depth the temperature of the Washington slab is estimated to be 800–900°C, i.e., in the range expected for the relatively young slab material that is subducted at the trench at present. At 250 km depth, slab temperature has increased only slightly to 1000–1100°C (Figure 7). The expression of the southern part of the slab under Oregon is weak (see WUS00 and BSE-NL in Figure 8). The variation in strength of the slab-related velocity anomalies is consistent with the decreasing age (and therefore increasing temperature) of the subducting plate from Washington to Oregon [*Atwater*, 1989].

[48] The two small-scale low-temperature anomalies under California (corresponding to circles 3 and 11 in Figure 4) are intriguing and have been noted in previous tomographic studies of California [e.g., *Benz and Zandt*, 1993; *Dueker et al.*, 1993]. The small dimensions and strong lateral thermal gradient of over 2°C/km at a depth of 110 km implies that the anomalies have a relatively young (10–20 Ma) origin. Young age and small lateral extent of the anomalies seem more consistent with the signature of a convective instability [*Zandt and Carrigan*, 1993] than of a part of the Farallon plate [*Benz and Zandt*, 1993], which would have subducted at 20–30 Ma.

[49] High temperatures of 1100–1300°C at 50 km depth under the California Coast Ranges just south of the Mendocino Triple Junction (location of circle 4 in Figure 4) are inferred from NA00 + WUS00 and from BSE-NL. Such temperatures are consistent with the evolution of a shallow slabless window under the Coast Ranges, as the triple junction migrates northward [*Lachenbruch and Sass*, 1980].

6. Discussion

6.1. Fluid Content

[50] The large discrepancy between T_P and T_S under the Cascades described in the section 5.1 was attributed to the presence of fluids. Using published partial derivatives of velocity variations in response to the presence of fluids/melt a first-order estimate of the amount of fluids present can be made. If we assume that the temperatures inferred from V_P and heat flow are a reasonable approximation of the thermal state of the mantle under the Cascades, a 9–13% low shear velocity anomaly has to be explained by the presence of fluids. This nonthermal δV_S corresponds to a 1.5–2.0% fluid fraction using the derivatives of *Hammond and Humphreys* [2000]. Estimates of $\partial \ln V_S/\partial \ln V_P$ for the effect of fluids range between 2 and 2.3 [*Goes et al.*, 2000; *Hammond and Humphreys*, 2000]. This relative sensitivity of V_S and V_P to fluids/melt is not different enough from the relative sensitivity to temperature, $\partial \ln V_S/\partial \ln V_P$ = 1.3–2.0 [*Goes et al.*, 2000], to explain the very strong V_S anomaly and the mild V_P anomaly under the Cascades. However, $\partial \ln V_S/\partial \ln V_P$ could be larger if the effect of fluids on melting temperature leads to a lowering of Q_S [*Karato and Jung*, 1998]. Thus it seems likely that part of the difference between the T_P and T_S estimates obtained under the Cascades is due to the presence of fluids, but some of the discrepancy may be attributable to imaging effects on V_P and/or V_S.

The difference between T_P and T_S under the Gulf of California gives similar estimates of 1.5–2.0% for the melt and fluid content. Under the Basin and Range a maximum estimate of the fluid/melt content of 1.3% is obtained when Q_1 is used to determine the thermal contribution to $\partial \ln V_S / \partial \ln V_P$. However, the difference between T_P and T_S under the Basin and Range is relatively small (Figure 7) and may be close to zero if the Q_2 model applies (Figure 3), thus not requiring any fluids to explain V_P and V_S simultaneously.

6.2. Isostasy

[51] Although isostatic effects of variations in crustal structure can account for a significant part of surface topography there are discrepancies, especially in the continents and specifically under North America [*Humphreys and Dueker*, 1994a; *Mooney et al.*, 1998; *Lowry et al.*, 2000] that are generally attributed to shallow upper mantle structure. We modeled Airy isostatic uplift for North America, using the crustal structure from CRUST5.1 [*Mooney et al.*, 1998], and the mantle density structure from the thermal models derived from NA00 and BSE-NL.

[52] Thermal mantle structure down to 250 km depth inferred from NA00 predicts a difference in topography of ~1.5 km between the Basin and Range in Nevada and the Midcontinent. For a primitive garnet peridotite composition the thermal structure leads to a difference in average mantle density between 3380 and 3450 kg/m^3. When the effect of crustal structure (i.e., density and thickness) from CRUST5.1 [*Mooney et al.*, 1998] is added, the difference in topography increases to ~3 km (Figure 9). The highest elevations are now predicted in the south and central Rocky Mountains due to the combination of thick crust and relatively warm mantle and the predicted elevation of Nevada is ~2 km above the Midcontinent. The large-scale differences in topography predicted by isostatic compensation of crust and thermal mantle density structure agree quite well with the observed topography for most of the continent, with the exception of two areas (Figure 9). In the modeled elevation the Canadian Shield/northern part of the North American craton lies ~1 km too low relative to the Midcontinent south of the Great Lakes and the coastal regions of the Gulf of Mexico lie ~1 km too high (Figure 9b). The low model elevation of the Canadian Shield is the effect of dense cold mantle that is only partially compensated for by the crust, which is only 30 km thick as opposed to ~40 km under the Midcontinent. Thus an additional source of buoyancy is necessary to increase model elevations. Such buoyancy can be easily supplied by a more depleted mantle composition of the lithosphere under the Canadian shield than under the rest of the continent [*Jordan*, 1979]. We estimate that a decrease in iron content of 1% (from Mg number 89 to 90) over the depth range from the Moho to 250 km depth is sufficient to elevate the Canadian craton by 1 km. As only the integrated effect can be estimated, a stronger depletion, as often found in xenoliths [*Griffin et al.*, 1999], over a smaller depth range is equally possible. The high predicted elevations of the Gulf of Mexico and the gulf coast may be due to the use of a crustal thickness that is too large. The more detailed crustal model of *Chulick and Mooney* [1998] has a thinner crust in the gulf region than the 40 km thickness given in CRUST5.1. Structure below the compensation depth assumed in our isostatic calculation, e.g., from the cold Farallon lithosphere at 300–400 km depth [*van der Lee and Nolet*, 1997a] could also contribute to the lower than predicted elevation.

[53] We find that down to at least 250 km depth the mantle under the Basin and Range Province is on average 200°C warmer than the surrounding continental mantle (Figures 2 and 7). This relative variation in temperature together with CRUST5.1 is sufficient to account for the gross features of the relative elevations within the western United States. That is, our thermal mantle structure can explain the elevation of the Basin and Range relative to coastal California and the elevation of the Basin and Range relative to the Rocky Mountains. The high temperatures readily explain the over 2 km of mantle-induced topography that *Lowry et al.* [2000] infer under the center of the U.S. Basin and Range Province. *Kaban and Mooney* [2001] also find a strong low mantle density anomaly in about the same location. The low velocities related to these high temperatures persist no deeper than 350–400 km [*van der Lee and Nolet*, 1997a].

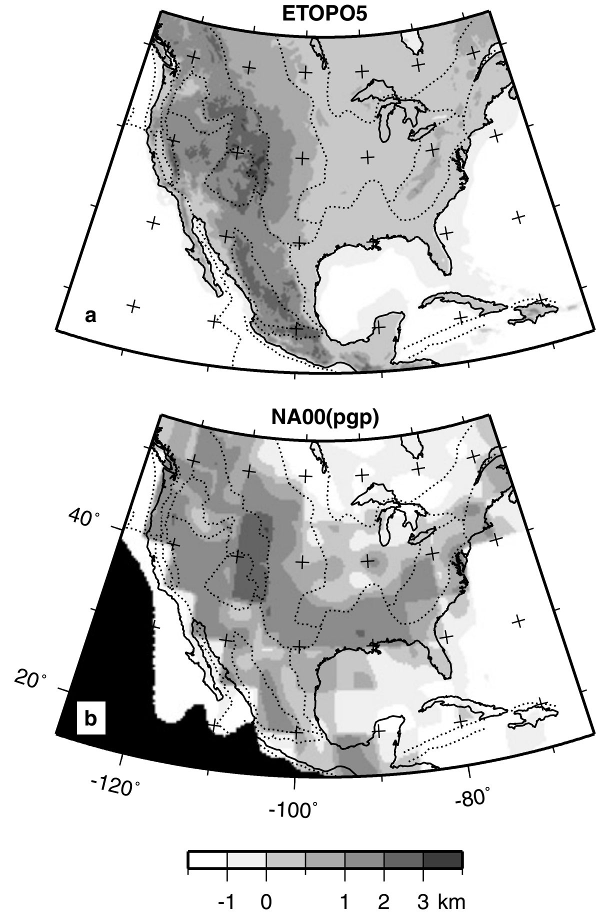

Figure 9. (a) Observed North American topography from ETOPO5 [*National Geophysical Data Center*, 1988] and (b) isostatic topography calculated from the NA00 thermal mantle structure down to 250 km using an undepleted (pgp, Table 1) composition and CRUST5.1 [*Mooney et al.*, 1998] crustal density structure. As a reference profile, a mid-oceanic ridge at a water depth of 2.5 km was used. Note that for western North America the relative topography is modeled quite well by thermally controlled mantle density variations and variations in crustal structure. This is not true under eastern North America, where T_S gives mantle densities that are too large under the Canadian cratonic part to explain observed topography and densities that are too small under the coastal region of the Gulf of Mexico.

7. Conclusions

[54] Observational constraints on the thermal state of the lithosphere have traditionally been surface heat flow measurements. This work and other recent efforts [e.g., *Sobolev et al.*, 1996; *Koper et al.*, 1999; *Goes et al.*, 2000; *Roth et al.*, 2000] show that seismic velocity models are starting to be well-enough resolved to provide an alternative source of information of

temperatures not only in the lithosphere but also below the lithosphere. Under most of North America, temperatures inferred from tomographic models for V_P and V_S agree within ±150°C. Uncertainties in experimental elastic and anelastic parameters and in seismic velocities do not allow us to constrain absolute temperatures from seismic velocities any tighter than ±150°C, although lateral temperature differences are better determined. The range in seismically estimated temperatures for the North American lithosphere agrees well with the range derived from surface heat flow measurements. The agreement between the three independent temperature estimates (from V_P, V_S, and heat flow) confirms that variations in shallow mantle seismic velocities are mainly the result of variations in temperature.

[55] We find that mantle temperatures at 50–100 km depth under the western United States are on average 500°C higher than under eastern North America. The thermal thickness of the lithosphere (defined as the depth of the 1200°C isotherm) is only 50 km or less under the Basin and Range, Rio Grande Rift and the eastern part of the Snake River Plain. The thermal lithosphere under the North American craton near the border with Canada is 200–250 km thick. Minimum temperatures under the craton are 400–500°C at 50 km depth, while temperatures in stable eastern North America away from the craton are 700–1000°C at 50 km depth. In the absence of any tectonic activity in interior eastern North America over the last 1 Gyr the observed variations in lithospheric temperature may be sustained by variations in lithospheric thickness that are a relict of Precambrian tectonics and are compositionally or rheologically stabilized. Isostatic calculations that account for crustal structure and thermal mantle structure down to 250 km depth yield elevations for the Canadian Shield that are 1 km below the elevation of the Midcontinent, while observed topography is no more than a few hundred meters. Additional buoyancy of the lithospheric mantle of the Canadian craton equivalent to an average 1% depletion in iron over a 50–250 km depth range eliminates the difference in modeled isostatic elevation.

[56] Under the western United States the regional velocity model WUS00 complements NA00 and BSE-NL with information on smaller-scale (50–100 km) velocity structure. Low seismic velocities under the Basin and Range that continue down to 300–400 km depth give temperatures following a 1300°C mantle adiabat in the 50–250 km depth range we investigated. Within the ±150°C uncertainties none of the temperatures under the western United States exceed the mantle adiabat, but they are around 200°C higher than the temperatures of the surrounding continental mantle. Widespread melting is not required to reconcile *P* and *S* wave velocities under the western United States, but small-scale velocity anomalies indicate that locally ~1% melt could be present, for example, under the southwestern edge of the Colorado Plateau, parts of the Rio Grande Rift, and under Yellowstone. The high temperatures under western North America over a depth range of 250 km are sufficient to account for the long-wavelength high topography of the western part of the continent and variations in mantle temperature together with variations in crustal structure can account for the relative elevations. Under the Cascades and the Gulf of California, *S* wave velocities between 50 and 100 km depth provide evidence for the presence of 1–2% fluids (water and melt) on a larger scale. The discrepancies in temperatures inferred from V_P and V_S under the Wyoming craton and extending toward the Colorado Plateau are enigmatic and cannot easily be explained by either hydration or anisotropy.

[57] **Acknowledgments.** We are very grateful to Ken Dueker and Wim Spakman for allowing us to use their most recent velocity models and for their comments on our interpretation of the models. We thank Walter Mooney for providing his database on North American crustal structure for this study and for many interesting discussions. Stephan Sobolev's and Walter Mooney's thorough reviews stimulated improvements of the manuscript. All figures were drawn using GMT [*Wessel and Smith*, 1995]. Contribution 1203 of the Institute of Geophysics, ETH Zurich.

References

Artemieva, I. M., Evolution of deep thermal regime of the Western U.S.A.: Evidence of Cenozoic magmatism, *Eos Trans. AGU*, *77*(46), Fall Meet. Suppl., F666, 1996.

Artemieva, I. M., and W. D. Mooney, Thermal thickness and evolution of Precambrian lithosphere: A global study, *J. Geophys. Res.*, *106*, 16,387–16,414, 2001.

Atwater, T., Plate tectonic history of the northeast Pacific and western North America, in *The Geology of North America*, vol. N, *The Eastern Pacific Ocean and Hawaii*, pp. 21–72, Geol. Soc. of Am., Boulder, Colo., 1989.

Bass, J. D., Elasticity of minerals, glasses, and melts, in *Mineral Physics and Crystallography: A Handbook of Physical Constants*, *AGU Ref. Shelf*, vol. 2, edited by T. J. Ahrens, pp. 45–63, AGU, Washington, D. C., 1995.

Benz, H. M., and G. Zandt, Teleseismic tomography: Lithospheric structure of the San Andreas Fault system in northern and central California, in *Seismic Tomography: Theory and Practice*, edited by H. M. Iyer and K. Hirahara, pp. 440–465, Chapman and Hall, New York, 1993.

Berckhemer, H., et al., Shear modulus and *Q* of forsterite and dunite near partial melting from forced oscillation experiments, *Phys. Earth Planet. Inter.*, *29*, 30–41, 1982.

Bijwaard, H., and W. Spakman, Non-linear global *P*-wave tomography by iterated linearized inversion, *Geophys. J. Int.*, *141*, 71–82, 2000.

Bijwaard, H., W. Spakman, and E. R. Engdahl, Closing the gap between regional and global travel time tomography, *J. Geophys. Res.*, *103*, 30,055–30,078, 1998.

Braile, L. W., et al., Seismic properties of the crust and uppermost mantle of the conterminous United States and adjacent Canada, in *Geophysical Framework of the Continental United States*, edited by L. C. Pakiser and W. D. Mooney, *Mem. Geol. Soc. Am.*, *172*, 655–680, 1989.

Carlson, R. W., A. J. Irving, and B. C. Hearn Jr., Chemical and isostopic systematics of peridotite xenoliths from the Williams Kimberlite, Montana: Clues to processes of lithosphere formation, modification, and destruction, in *Proceedings of the 7th International Kimberlite Conference*, edited by J. J. Gurney et al., pp. 90–98, Red Roof Design, Cape Town, South Africa, 1999.

Chapman, D. S., Thermal gradients in the continental crust, in *The Nature of the Lower Continental Crust*, edited by J. B. Dawson et al., *Geol. Soc. Spec. Publ.*, *25*, 63–70, 1986.

Chulick, G. S., and W. D. Mooney, New maps of North American crustal structure, *Seismol. Res. Lett.*, *69*, 160, 1998.

Decker, E. R., Thermal regimes of the Southern Rocky Mountains and Wyoming Basin in Colorado and Wyoming in the United States, *Tectonophysics*, *244*, 85–106, 1995.

Dickinson, W. R., and W. S. Snyder, Geometry of subducted slabs related to San Andreas Transform, *J. Geol.*, *87*, 609–627, 1979.

Dueker, K., E. Humphreys, and G. Biasi, Teleseismic imaging of the western U.S. upper mantle structure using the simultaneous iterative reconstruction technique, in *Seismic Tomography: Theory and Practice*, edited by H. M. Iyer and K. Hirahara, pp. 265–298, Blackwell, Malden, Mass., 1993.

Dueker K., H. Yuan, and B. Zurek, Thick-structure Proterozoic lithosphere of the Rocky Mountain region, *GSA Today*, *11*(2), 4–9, 2001.

Dueker, K. G., New seismic images of the western U.S. from crust to 660 km, *Seismol. Res. Lett.*, *70*, 2, 1999.

Engdahl, E. R., R. D. van der Hilst, and R. P. Buland, Global teleseismic earthquake relocation with improved travel times and procedures for depth determination, *Bull. Seismol. Soc. Am.*, *88*, 722–743, 1998.

Goes, S., R. Govers, and P. Vacher, Shallow upper mantle temperatures under Europe from *P* and *S* wave tomography, *J. Geophys. Res.*, *105*, 11,153–11,169, 2000.

Grand, S. P., Mantle shear structure beneath the Americas and surrounding oceans, *J. Geophys. Res.*, *99*, 11,591–11,621, 1994.

Griffin, W. L., S. Y. O'Reilly, and C. G. Ryan, The composition and origin of subcontinental lithospheric mantle, in *Mantle Petrology: Field Observations and High-Pressure Experimentation: A Tribute to Francis R. (Joe)* Boyd, edited by Y. Fei, *Spec. Publ. Geochem. Soc.*, *6*, 13–43, 1999.

Hammond, W. C., and E. D. Humphreys, Upper mantle seismic wave velocity: Effects of realistic partial melt geometries, *J. Geophys. Res.*, *105*, 10,975–10,986, 2000.

Henry, C. D., and J. J. Aranda-Gómez, The real southern Basin and Range: Mid- to late Cenozoic extension in Mexico, *Geology*, *20*, 701–704, 1992.

Hirth, G., and D. L. Kohlstedt, Water in the oceanic upper mantle: Implications for rheology, melt extraction and the evolution of the lithosphere, *Earth Planet. Sci. Lett.*, *144*, 93–108, 1996.

Humphreys, E. D., and K. G. Dueker, Physical state of the western U.S. upper mantle, *J. Geophys. Res.*, *99*, 9635–9650, 1994a.
Humphreys, E. D., and K. G. Dueker, Western U.S. upper mantle structure, *J. Geophys. Res.*, *99*, 9615–9634, 1994b.
Iwamori, H., and D. Zhao, Melting and seismic structure beneath the northeast Japan arc, *Geophys. Res. Lett.*, *27*, 425–428, 2000.
Jordan, T. H., Mineralogies, densities and seismic velocities of garnet lherzolites and their geophysical implications, in *The Mantle Sample: Inclusions in Kimberlites and Other Volcanics*, edited by F. R. Boyd and H. O. A. Myer, pp. 1–14, AGU, Washington, D. C., 1979.
Kaban, M. K., and W. D. Mooney, Density structure of the lithosphere in the southwestern United States and its tectonic implications, *J. Geophys. Res.*, *106*, 721–739, 2001.
Kane, M. F., and R. H. Godson, A crust/mantle structural framework of the conterminous United States based on gravity and magnetic trends, in *Geophysical Framework of the Continental United States*, edited by L. C. Pakiser and W. D. Mooney, pp. 383–403, Geol. Soc. of Am., Boulder, Colo., 1989.
Karato, S., Importance of anelasticity in the interpretation of seismic tomography, *Geophys. Res. Lett.*, *20*, 1623–1626, 1993.
Karato, S., and H. Jung, Water, partial melting and the origin of the seismic low velocity and high attenuation zone in the upper mantle, *Earth Planet. Sci. Lett.*, *157*, 193–207, 1998.
Karato, S., and H. A. Spetzler, Defect microdynamics in minerals and solid-state mechanisms of seismic wave attenuation and velocity dispersion in the mantle, *Rev. Geophys.*, *28*, 399–421, 1990.
Koper, K. D., et al., Constraints on the origin of slab and mantle wedge anomalies in Tonga from the ratio of *P* and *S* velocities, *J. Geophys. Res.*, *104*, 15,089–15,104, 1999.
Lachenbruch, A. H., and J. H. Sass, Heat flow and energetics of the San Andreas Fault zone, *J. Geophys. Res.*, *85*, 6185–6222, 1980.
Lachenbruch, A. H., J. H. Sass, and P. Morgan, Thermal regime of the southern Basin and Range Province, 2, Implications of heat flow for regional extension and metamorhphic core complexes, *J. Geophys. Res.*, *99*, 22,121–22,133, 1994.
Lowry, A. R., N. M. Ribe, and R. B. Smith, Dynamic elevation of the Cordillera, western United States, *J. Geophys. Res.*, *105*, 23,371–23,390, 2000.
McDonough, W. F., Constraints on the composition of the continental lithospheric mantle, *Earth Planet. Sci. Lett.*, *101*, 1–18, 1990.
McKenzie, D., and M. J. Bickle, The volume and composition of melt generated by extension of the lithosphere, *J. Petrol.*, *29*, 625–679, 1988.
Mooney, W. D., G. Laske, and T. G. Masters, CRUST5.1: A global crustal model at 5° × 5°, *J. Geophys. Res.*, *103*, 727–747, 1998.
Morgan, P., and W. D. Gosnold, Heat flow and thermal regimes in the continental United States, in *Geophysical Framework of the Continental United States*, edited by L. C. Pakiser and W. D. Mooney, pp. 493–522, Am. Geol. Soc. of Am., Boulder, Colo., 1989.
National Geophysical Data Center, Digital relief of the surface of the Earth, Natl. Oceanic and Atmos. Admin., Boulder, Colo., 1988.
Nolet, G., and A. Zielhuis, Low *S* velocities under the Tornquist-Teisseyre zone: Evidence for water injection into the transition zone by subduction, *J. Geophys. Res.*, *99*, 15,813–15,820, 1994.
Nolet, G., C. Coutlee, and B. Clouser, *Sn* velocities in western and eastern North America, *Geophys. Res. Lett.*, *25*, 1557–1561, 1998.
Pollack, H. N., and D. S. Chapman, On the regional variation of heat flow, geotherms and lithospheric thickness, *Tectonophysics*, *38*, 279–296, 1977.
Pollack, H. N., S. J. Hurter, and J. R. Johnson, Heat flow from the Earth's interior: Analysis of the global data set, *Rev. Geophys.*, *31*, 267–280, 1993.
Roth, E. G., D. A. Wiens, and D. Zhao, An empirical relationship between seismic attenuation and velocity anomalies in the upper mantle, *Geophys. Res. Lett.*, *27*, 601–604, 2000.
Schmeling, H., Numerical models on the influence of partial melt on elastic, anelastic and electric properties of rocks, part 1, Elasticity and anelasticity, *Phys. Earth Planet. Inter.*, *41*, 34–57, 1985.
Simkin, T., and L. Siebert, *Volcanoes of the World*, 386 pp., Geoscience, Tucson, Ariz., 1994.
Sobolev, S. V., and A. Y. Babeyko, Modeling of mineralogical composition, density and elastic wave elocities in anhydrous magmatic rocks, *Surv. Geophys.*, *15*, 515–544, 1994.
Sobolev, S. V., et al., Upper mantle temperatures from teleseismic tomography of French Massif Central including effects of composition, mineral reactions, anharmonicity, anelasticity and partial melt, *Earth Planet. Sci. Lett.*, *139*, 147–163, 1996.
Sobolev, S. V., A. Grésillaud, and M. Cara, How robust is isotropic delay time tomography for anisotropic mantle, *Geophys. Res. Lett.*, *26*, 509–512, 1999.
Thompson, A. B., Water in the Earth's upper mantle, *Nature*, *358*, 295–302, 1992.
van der Lee, S., and G. Nolet, Seismic image of the subducted trailing fragments of the Farallon plate, *Nature*, *386*, 266–269, 1997a.
van der Lee, S., and G. Nolet, Upper mantle *S* velocity structure of North America, *J. Geophys. Res.*, *102*, 22,815–22,838, 1997b.
van der Lee, S., D. James, and P. Silver, Upper mantle *S* velocity structure of central and western South America, *J. Geophys. Res.*, *106*, 30,821–30,834, 2001.
Wessel, P., and W. H. F. Smith, New version of the generic mapping tools released, *Eos Trans. AGU*, *76*, 329, 1995.
Zandt, G., and C. R. Carrigan, Small-scale convective instability and upper mantle viscosity under California, *Science*, *261*, 460–463, 1993.

S. Goes and S. van der Lee, Institute of Geophysics, ETH Hönggerberg (HPP), CH-8093 Zurich, Switzerland. (saskia@tomo.ig.erdw.ethz.ch; suzan@tomo.ig.erdw.ethz.ch)

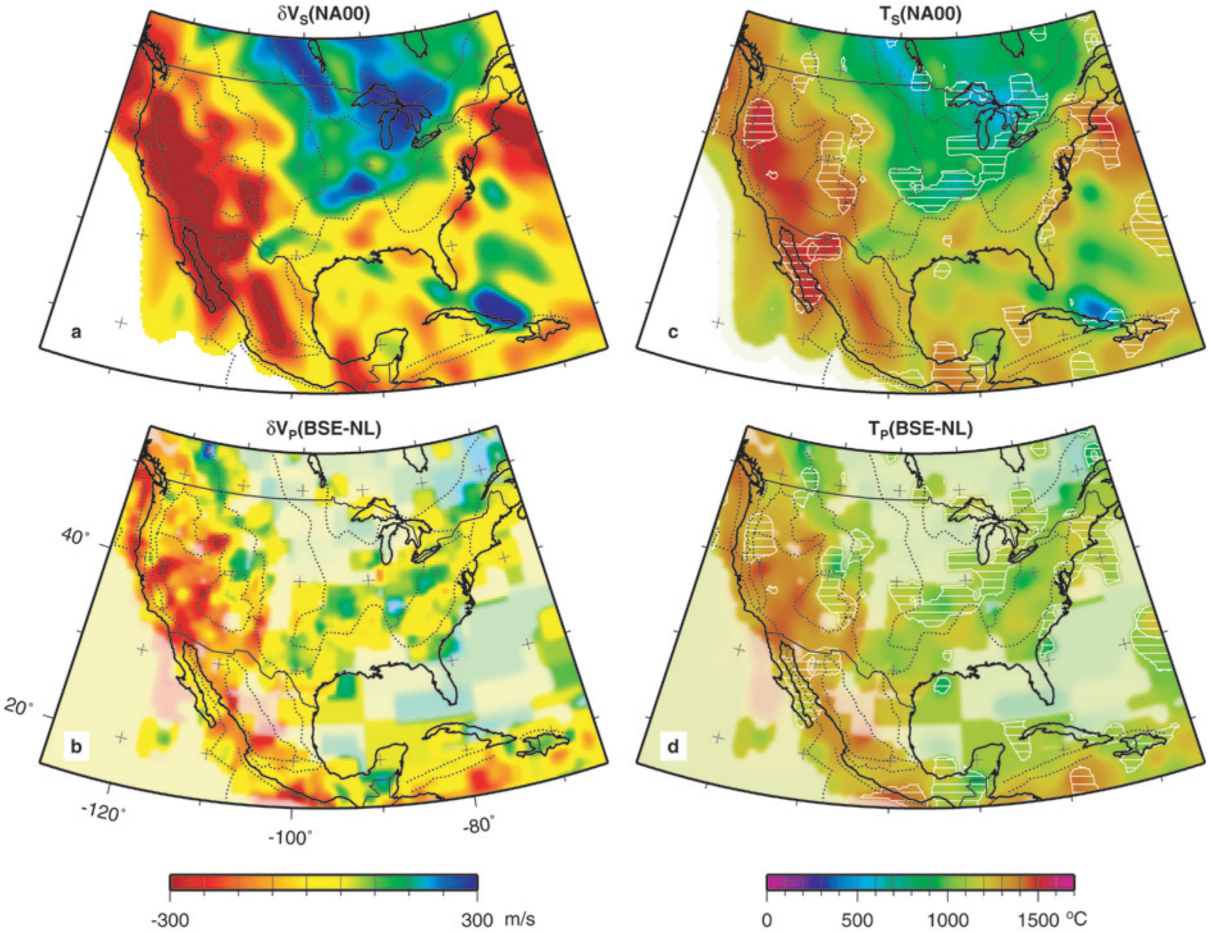

Figure 2. Maps of velocities and temperatures at 110 km depth. (a) Shear wave velocities from model NA00 [*van der Lee and Nolet*, 1997b] relative to a reference velocity of 4.5 km/s. (b) Compressional wave velocities from model BSE-NL [*Bijwaard and Spakman*, 2000] relative to reference model ak135 (8.05 km/s at this depth). Colors in Figures 2b and 2d are faded where the hit count of BSE-NL is below 200 and resolution deemed low. Velocity anomalies are shown in m/s. Note that on a percent scale, *S* velocity anomalies would be about twice as strong as *P* velocity anomalies. (c) Temperatures estimated from NA00. (d) Temperatures inferred from BSE-NL. Both thermal models were smoothed over a length scale of 300 km using a moving Gaussian window. Temperatures may be unreliable in the hatched regions where T_S and T_P differ by more than 150°C. The acgl composition and Q_1 anelasticity model were used for the interpretation of the seismic velocities.

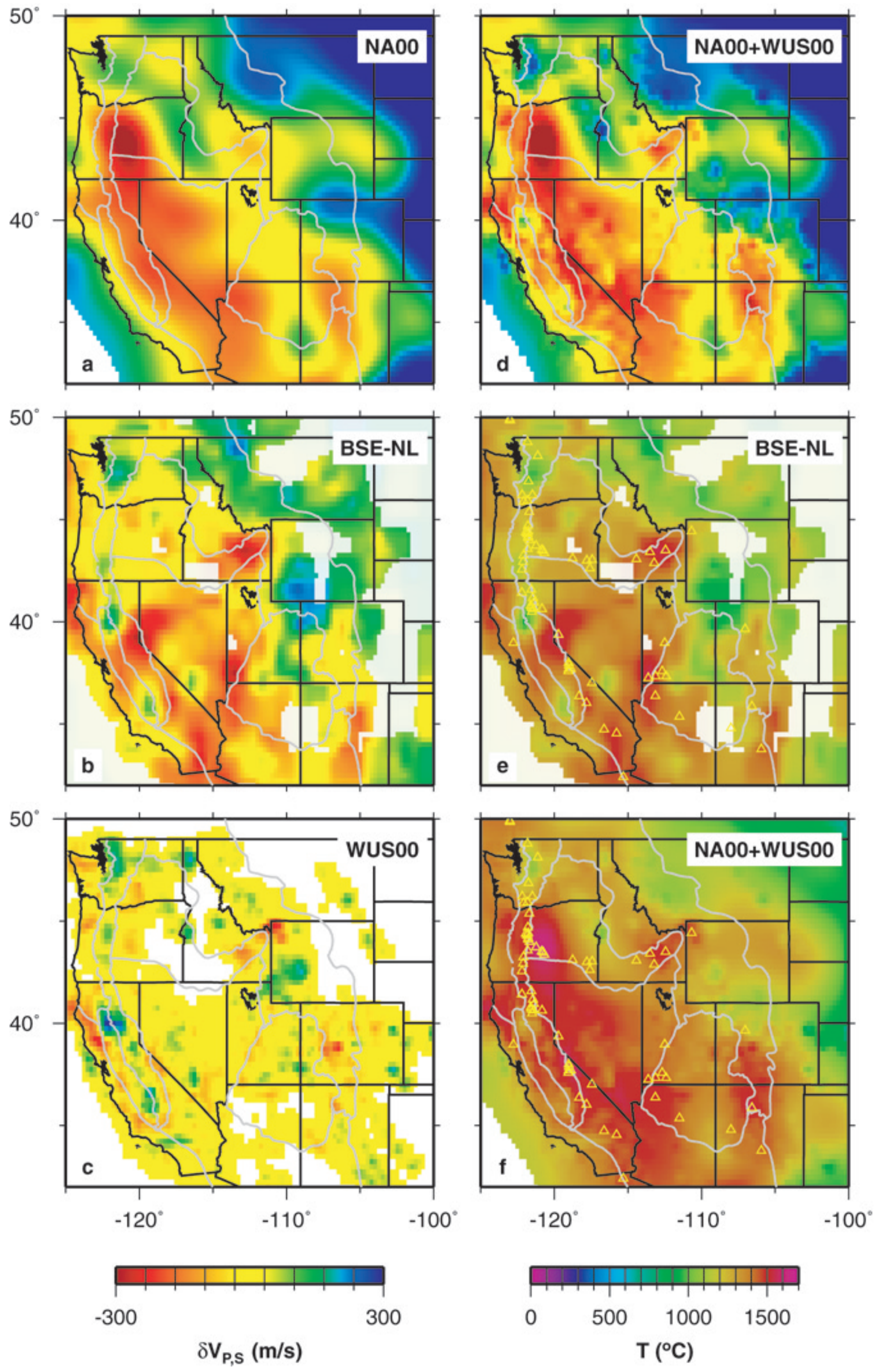

Figure 8. Maps at 110 km depth for the western United States for the three velocity models NA00 (V_S), BSE-NL (V_P), WUS00 (V_P) and a composite model of NA00 and WUS00 (V_S) and temperatures inferred from the composite V_S model and BSE-NL for the acgl composition and Q_1 anelasticity model. Velocity anomalies are shown in m/s relative to the average velocity in this region ($V_P = 4.29$ km/s, $V_S = 7.99$ km/s). Areas where no velocities are resolved are left white. Gray lines mark physiographic boundaries, black lines state boundaries (courtesy of K. Dueker). Yellow triangles show the location of Holocene volcanoes [*Simkin and Siebert*, 1994].